Oxidation Behaviour and Rim Formation Mechanism of Tungsten Electrode†

Fukuhisa MATSUDA*, Masao USHIO** and Alber A. SADEK***

Abstract

The oxidation behaviour and vaporization of tungsten electrode activated with La_2O_3 (2%) during arcing was measured and compared in $Ar + O_2$ mixtures containing 0.2% oxygen and pure argon at 1 atm total pressure. The presence of oxygen in shielding gas enhances the vaporization rate of tungsten and forming rim.

Theoretical studies were carried out to evaluate the oxidation and vaporization rates of tungsten. The rates generally decreases with increasing temperature, i.e. in the direction to the electrode tip. Investigation by SEM and direct observation of arc were carried out to observe the formation steps, structure and the location of rim The experimental results are in reasonable agreement with theoritical studies.

The formation mechanism of rim was attributed to the vaporization, dessociation and deposition phenomenas of tungsten oxides which occured simultaneously along the electrode surface during arcing.

KEY WORDS: TUNGSTEN, TUNGSTEN OXIDES, GTA WELDING, TUNGSTEN VAPORIZATION

1. Introduction

As shown before[1] in these series of papers that, the contamination of shielding gas by oxidizing component leads to failure of electrode and formation of rim.

There are several mechanisms of rim formation[2], but until now there is no clear-cut explenation of this phenomena. The aim of this study is to explain the formation mechanism of rim theoretically and experimentally by following up the rim formation. The theoretical studies were based on the volatility charactaristics of tungsten oxides and the motion of these oxides along the electrode surface.

2. Theoretical Calculations

There are many theories studied the vaporization of metals in a stream of inert gas with or without presence of oxidizing elements at different pressures[3-7]. All of these studies were carried out on metal plates, thin wires and/or rods. Also, the heated subjects were resistively heated using a constant current supply for constant temperatures. But in case of GTAW electrodes, the heating source is the arc itself which leading to very high temperature gradient along the electrode surface. Also, the geometry of electrode is quiet different than the geometry of plate or cylinderical wires,...etc.

Then, it is necessary to correlats the basic dimensionless parameters of transport equations of shielding gas and make another derivation of rate equation for vaporization in a temperature gradient.

2-1 Transport Properties of Gases and Metal Vapors

As discussed before[8], the transport properties of gases, can be predicted theoritically on the basis of the rigorous kinetic theory of gases.

In all the transport properties given below, the collision diameter and collision integral for gases are those based on the intermolecular Lennard-Jones potential energy function[9]. The collision diameter for the volatile oxide species can be obtained from the known geometry of various molecules[10] and using Equ. (1) to calculate the collision radius[11].

$$r_{A_mB_n} = (m\, r_A^3 + n\, r_B^3)^{1/3} \qquad (1)$$

For collision between unlike molecules of species 1 and 2 the collision diameter is taken as the arithmetical mean

† Received on Nov. 4, 1987
* Professor
** Associate Professor
*** Graduate Student, Osaka University.

Transactions of JWRI is published by Welding Research Institute of Osaka University, Ibaraki, Osaka 567, Japan

of the components thus;

$$\sigma_{1,2} = \frac{\sigma_1 + \sigma_2}{2} \qquad (2)$$

and the maximum energy of attraction is approximated as the geometrical mean of the pure components, thus;

$$\epsilon_{1,2} = \sqrt{\epsilon_1 \epsilon_2} \qquad (3)$$

Using the force constants and k/ϵ (where k is the Boltzman's constant) and the collision integrals in reference(9), the transport properties can be calculated using the following equations derived from the kinetic theory of gases:

a) Binary Interdiffusivity

$$D_{1,2} = 2.628 \times 10^{-3} \frac{\sqrt{T^3 (M_1 + M_2)/2M_1M_2}}{P \cdot \sigma_{1,2}^2} \qquad (4)$$

where M is the molecular weight and P is the total pressure.

b) Coefficient of Viscosity(binary mixtures)

$$\mu_{1,2} = \frac{N_1\mu_1}{N_1\phi_{1,1} + N_2\phi_{1,2}} + \frac{N_2\mu_2}{N_1\phi_{2,1} + N_2\phi_{2,2}} \qquad (5)$$

where

$$\phi_{1,2} = \frac{1}{\sqrt{8}}\left(1 + \frac{M_1}{M_2}\right)^{-1/2} \left[1 + \left(\frac{\mu_1}{\mu_2}\right)^{1/2} \left(\frac{M_2}{M_1}\right)^{1/4}\right]^2$$

$$\phi_{1,2} = \frac{1}{\sqrt{8}}\left(1 + \frac{M_2}{M_1}\right)^{-1/2} \left[1 + \left(\frac{\mu_2}{\mu_1}\right)^{-1/2} \left(\frac{M_1}{M_2}\right)^{1/4}\right]^2$$

$\phi_{1,1} = \phi_{2,2} = 1$

N_1, N_2 = mole fraction of components 1 and 2.
μ_1, μ_2 = coefficient of viscosity of components 1 and 2

2.2 Correlation of Basic Dimensionless Parameters

For fast gas streams and in the presence of a temperature gradient allowance should be made for the variation of transport properties with temperature. Then these corrections are hardely necessary.

$$\bar{N}_u = 2 + 0.6\,[(G_r)^{1/4} + (R_e)^{1/2}]\,(S_c)^{1/3} \qquad (6)$$

where

N_u = Nusselt number.

G_r = Grashof number.

$$= \frac{g \cdot d^3}{\nu^3}\left(\frac{\rho_\infty}{\rho_s} 1\right) \qquad (7)$$

R_e = Reynolds number

$$= \frac{u\,d}{\nu} \qquad (8)$$

S_c = Schmidt number

$$= \frac{\nu}{D} \qquad (9)$$

g = acceleration of gravity
ν = kinematic viscosity = viscosity/density
ρ_∞, ρ_s = densities at T_∞ and T_s respectively.
u = gas velocity.
d = diameter.
D = interdiffusivity

2.3 Derivation of Rate Equation for Vaporization in Temperature Gradient

To make derivation of rate equation first a volatile oxide counter diffusion model can be constructed to explain the high temperature oxidation of tungsten. This model which is schematically shown in **Fig. 1** is assumed under the assumptions:

(1) the oxygen species which diffuse across the gaseous boundary and impinging on the tungsten surface is molecular oxygen.
(2) the equilibrium formation of volatile oxides of tungsten and monatomic oxygen at the metal surface.
(3) the counter diffusion of these species back across the boundary layer.
(4) there are no other homogenous chemical reactions in the boundary layer.

This model must be fulfilled the condition of conservation of oxygen and tungsten atoms, thus,

$$-2J_{O_2} = J_O + J_{WO} + 2J_{WO_2} + 3J_{WO_3} + 6J_{W_2O_6} + 8J_{W_3O_8} + 9J_{W_3O_9} \qquad (10)$$

$$\Sigma J_W = J_{WO} + J_{WO_2} + J_{WO_3} + 2J_{W_2O_6} + 3J_{W_3O_8} + 3J_{W_3O_9} \qquad (11)$$

where:

J = flux (mole/cm^2.s)
J_W = rate of tungsten volatilization.

A theoritical analysis of homogeneous chemical reactions would be extremly complex since, the calculations were carried out on four species diffusing in the boundary

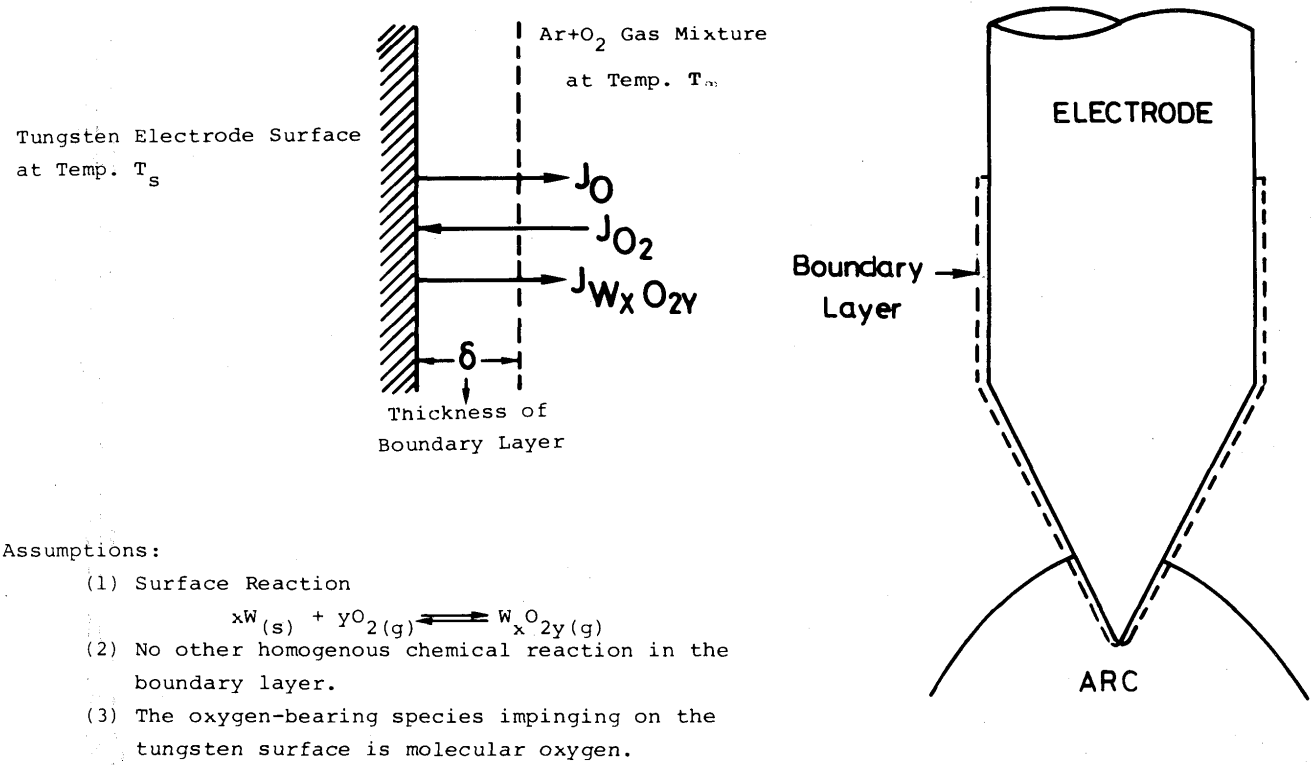

Assumptions:

(1) Surface Reaction

$$xW_{(s)} + yO_{2(g)} \rightleftharpoons W_xO_{2y(g)}$$

(2) No other homogenous chemical reaction in the boundary layer.

(3) The oxygen-bearing species impinging on the tungsten surface is molecular oxygen.

Fig. 1 Schematic illustration of volatile oxide counter diffusion model in Ar + O_2 atmosphere.

layer namely, WO, WO_2, WO_3 & W_2O_6.

Under the above boundary layer conditions, by Fick's law, the counter flux of tungsten vapor and oxygen will be as follow;

$$J_{o_2} = -\frac{D_{O_2,\,Ar}}{\Delta RT}(P_{O_2} - P'_{O_2}) \tag{12}$$

$$J_{W_xO_{2y}} = \frac{D_{W_xO_{2y},\,Ar}}{\Delta RT}(P_{W_xO_{2y}} - P'_{W_xO_{2y}}) \tag{13}$$

where

Δ = boundary layer parameter.

$D_{O_2,\,Ar}$ $D_{W_xO_{2y}}$ = binary diffusion coefficient of oxygen and tungsten oxide respictively in argon (cm^2/s).

P'_{O_2}, $P'_{W_xO_{2y}}$ = partial pressure of oxygen and tungsten oxide at the gas-metal interface (atm).

P_{O_2}, $P_{W_xO_{2y}}$ = partial pressure of oxygen and tungsten oxide in the bulk of the gas phase (atm).

T = temperaure (K).

The boundary layer prameter is given by

$$\Delta = d\,ln(1 + \delta/d) \tag{14}$$

where

d = radius of electrode (cm).

δ = boundary layer thickness (cm).

$$\delta = \frac{d}{N_u - 2} \tag{15}$$

Noting that, the temperature used in the evaluation of diffusivity as well as for boundary layer is the boundary layer reference temperature T_R given by the following equation,

$$T_R = T_S - 0.38\,(T_S - T_\infty) \tag{16}$$

where

T_S = electrode surface temperature (K)

T_∞ = ambient gas temperature (K)

Since there is equilibrium at the surface, it follows that,

$$K_{equ.} = \frac{P_{W_xO_{2y}}}{(P'_{O_2})^y} \tag{17}$$

By substituting $P'_{W_xO_{2y}}$ from Equ. (17) in Equ. (13) and noting that $P'_{W_xO_{2y}} \gg P_{W_xO_{2y}}$ the value of $J_{W_xO_{2y}}$ is obtained as follows;

$$J_{W_xO_{2y}} = \frac{(D_{W_xO_{2y},\,Ar})\,(K_{W_xO_{2y}})}{\Delta RT}\,(P'_{O_2})^y \quad (18)$$

Based on that, the rate equations for all volatile oxides can be obtained for any temperature and bulk oxygen pressure. But the resultant equations will contaion two unknowns, ΣJ_W and P'_{O_2}, provided that the diffusivities, boundary layer parameter are known from Equs. (4) and (14) respectivily.

The equilibrium constants can be obtained from the thermodynamics of W-O system[10], as follows,

$$K_{P_{W_xO_{2y}}} = e^{\frac{\Delta G^{\theta}_{W_xO_{2y}} + RT\ln P}{-RT}} \quad (19)$$

where

$\Delta G^{\theta}_{W_xO_{2y}}$ = standared oxidation free energy of tungsten oxide at 1 atm of oxygen (cal/mole)
P = bulk oxygen pressure (atm)
R = gas constant.

By substituting the various equilibrium constants and interdiffusivity in Equs. (10) and (11) gives us two equations with two unknowns (ΣJ_W and P'_{O_2}) which can be solved by iterative computation, giving the flux of tungsten oxide.

According to that, for a given temperature, the rate of vaporization of tungsten is expected to increase linearly with increasing partial pressure of oxygen. However, there is a restriction to this mechanism. This restriction is the maximum free vaporization can not be exceeded. By using Langmuir equation, the maximum vaporization rate in vacuo is given by,

$$J_{max} = \frac{P_i}{\sqrt{2\pi RTM_i}} \quad (20)$$

where P_i and M_i are the vapor pressure of metal (i) and molecular weight of the metal vapor, respectively.

When this limiting value of the flux is approached, the vaporization of tungsten oxide will cut-off.

That means, near this value of the flux, the vapor in contact with the metal surface is no longer saturated and thus the boundary condition assumed is no longer maintained, also δ approaches to the mean free path. Then the metal surface will be covered by a layer of liquide metal oxide. Since this metal oxide layer is in contact with metal at one interface and in contact with oxygen bearing species at the other interface, there is a sharp decrease in the vapor pressure of metal across the oxide layer. Then the rate of vaporization should become vanishingly small.

3. Experimental Work

To study the rim formation mechanism, W-La_2O_3 (2%) electrodes were used at various shielding gas mixtures, namely, pure argon, pure helium, argon + oxygen, argon + nitrogen and helium + oxygen. The choice of this kinde of electrodes was based on their least change in shape and structure and good arc characteristics as shown before[1].

The electrodes used in this work were produced by the conventional powder metallurgy process, with 3.2 mm in diameter, centerless ground. The shape of electrode tip is a cone angled at 45°. The effect of varying arc length and torch angle within sensible limits was assessed and found not to be alter the general trend of results. Therefore, a constant arc length of 3 mm and torch angle of 90° to the anode were used throghout this experimental work. The power source was a convential inverter TIG welding source, with direct current applied in electrode negative polarity and copper cooled anode.

The experimental procedures are as follows:

(1) Arcing with constant current in several gases had been done to measure the effect of shielding gases.

(2) Arcing with constant arc current at time intervals followed by weight change measurments had been done to observe the oxidation behaviour of these electrodes in Ar + O_2 gases in comparison with arcing in pure argon. The weight change measurments were carried out by using an electric balance with a sensitivity of 10^{-5} gm.

(3) Investigations by SEM and EDX analys were carried out in parallel with direct observation of the arc to observe the morphological changes and the distribution of La_2O_3 at the electrode surface with arcing time and current (direct observation method and apparatus were described in details in another paper in this issue).

4. Results and Discussion

4.1 Effect of Shielding gas

The appearance of electrode tip after 1 min arcing at 200A in different shielding gases are shown in **Fig. 2.** It is obvious that the presence of oxidizing element in shielding gas promote the rim formation accompanied with necking area just behind the rim. Moreover the size of rim and necking area is changed as a function of oxygen content as shown in the figure.

The most favorable mechanism for necking formation was thought as follows; after the rim formed the gas flow pattern changed from linear flow to circulation flow just behined the rim. This circulation flow increase the erro-sion rate of electrode at this region and forming this

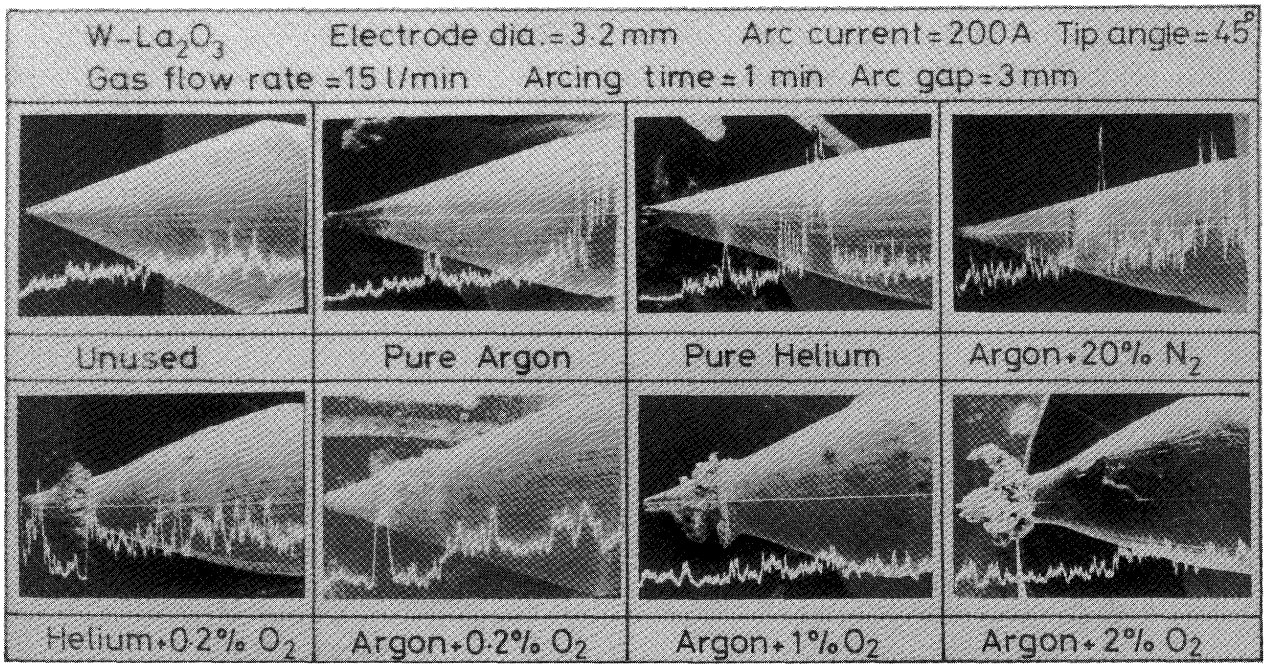

Fig. 2 Apperance of electrode surface after arcing in several shielding gases.

necking area.

Also Fig. 2 shows the distribution of La_2O_3 along the electrode tip, before and after usage. It is clearly observed that the La_2O_3 distribution was changed and concentrated in some places depending on the type of shielding gas. But in case of high content of oxygen in shielding gas the quantitative distribution of La_2O_3 is significantly changed and becomes vanishingly small. This is may be attributed to the higher temperature in that case.

4.2 Oxidation-Behaviour of Electrode During Arcing

As mentioned before, the oxidation of the present electrode, was traced in terms of weight change at time intervals. Such variation observed is a function of arc current and shielding gas.

In the following, the data are graphically presented for both pure argon and argon + oxygen shielding gases, **Figs. 3 and 4,** to observe the oxidation behaviour of tungsten electrode in oxidizing shielding gas. Fig. 3 shows the change in weight in pure argon with arcing time at 100 and 200A. It can be observe three stages of weight change with time as follows:

(1) At first arcing period weight decrease due to the rapidly vaporization of tungsten.
(2) After that, deposition occured on electrode surface leading to increase in weight.
(3) With prolonged time, temperature increased and the rate of vaporization is higher than the rate of deposition and the net rate of weight loss increase.

But in case of oxidizing shielding gas the mechanism of oxidation changes significantly as shown in Fig. 4, as follows:

(1) At first arcing period the oxide scale forms on the surface leading to weight increase.
(2) After that, the molar vaporization rate of tungsten oxide exceeds the molar consumption rate of metal leading to weight loss.
(3) With longe time, oxide disscociate and deposite and the net rate of metal loss decrease.

4.3 Rim Formation Steps

The rim formation was observed directly during arcing in Ar + 0.2%O_2 mixturte at 100 and 200A and showed in **Figs. 5 and 6** respectively. It is obvious that, the size and shape of rim depende on arcing time at given arc current. Also, the rate of rim formation depend on the arc current.

The formation steps of rim was observed by using SEM at intervals of arcing time and showed in **Fig. 7.** It is clearly observed that the rim formation steps are typically dendritic growing up steps.

4.4 Calculation Results

As mentioned before, that, the calculations were carried out on only 4 species of tungsten oxides, namely, WO, WO_2, WO_3 & W_2O_6 for the complexity of theoretical analysis of tungsten oxides. By using the boundary layer conditions which explained before and the temperature

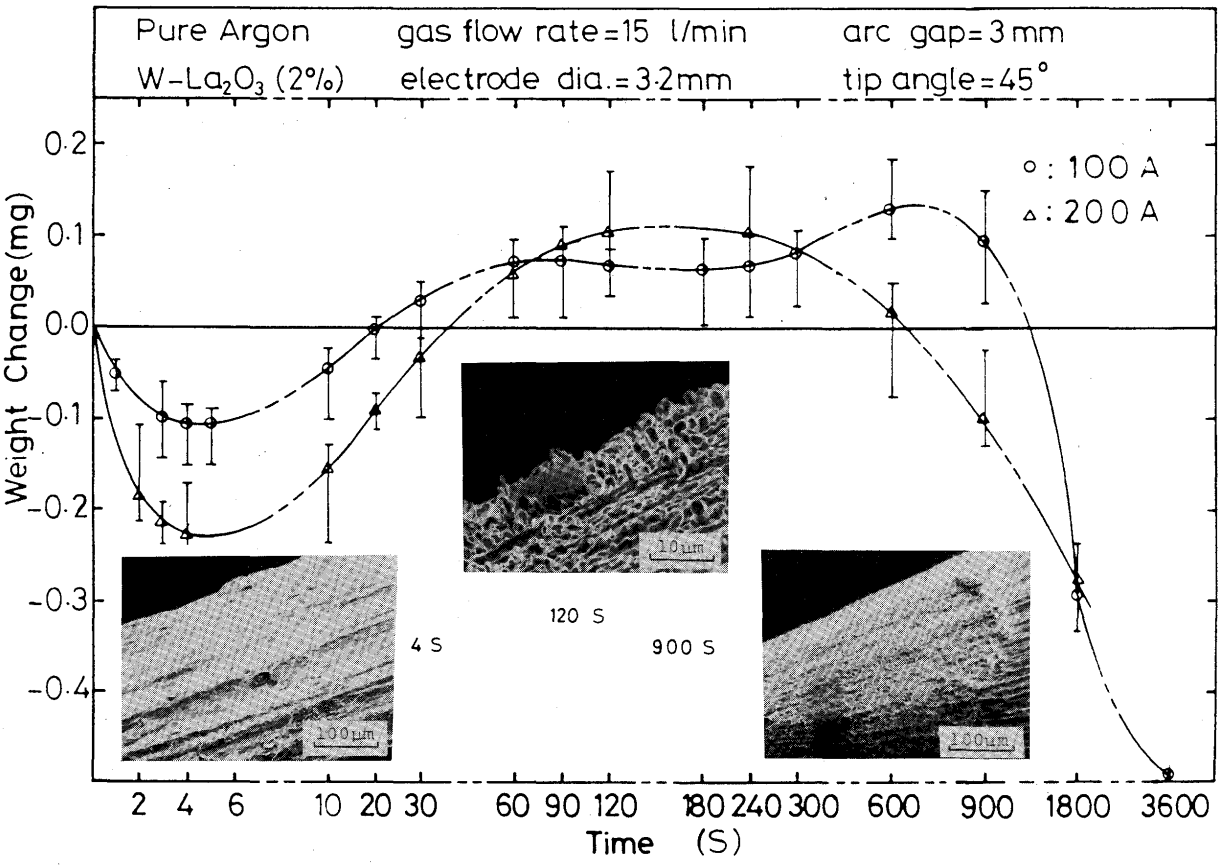

Fig. 3 Weight change due to arcing in pure argon at 100 and 200A of W-La_2O_3(2%) electrode.

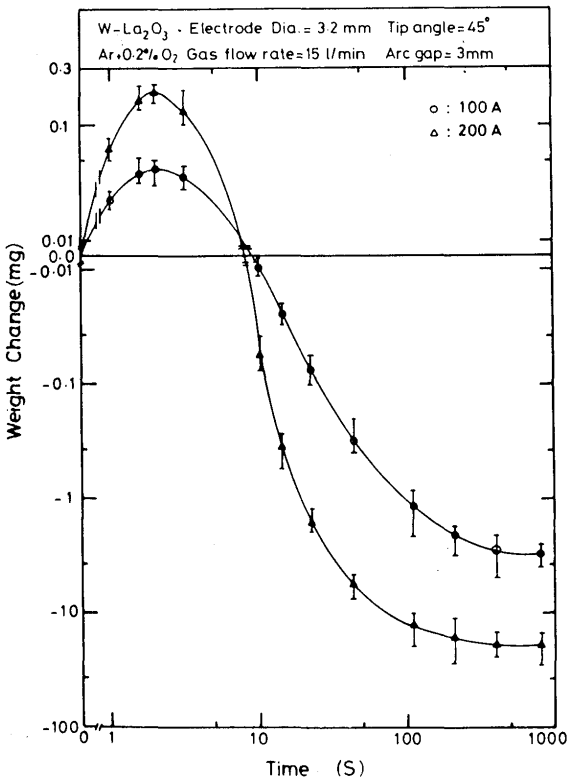

Fig. 4 Weight change due to arcing in Ar + 0.2%O_2 at 100 and 200A of W-La_2O_3(2%) electrode.

distribution on the electrode surface which measured previously[13], a computer program can be constructed to calculate the total flux of vaporized tungsten oxides. The following resultes were obtained and showed in **Fig. 8.**

The important features of the data in Fig. 8 are as follows:

(1) The rate of vaporization generally decreases with increasing temperature. In other words, at the electrode surface there is a very high temperature gradient due to arcing, then the rate of oxidation and vaporization of oxides first increase until maximum value and then decrease to minimum value through the direction to the electrode tip at which there is the higher temperature zone.

The decrease in oxidation and vaporization rate with increasing temperature can be understood by considering Equ. (11) and the flux equation for every tungsten oxide in more detail, as follows; by using an average binary diffusion coefficient for all volatile oxides ($\bar{D}$), then Equ. (11) becomes

$$\Sigma J_W = \frac{\bar{D}}{\Delta RT}(P_{WO} + P_{WO_2} + P_{WO_3} + 2P_{W_2O_6}) \quad (21)$$

Or

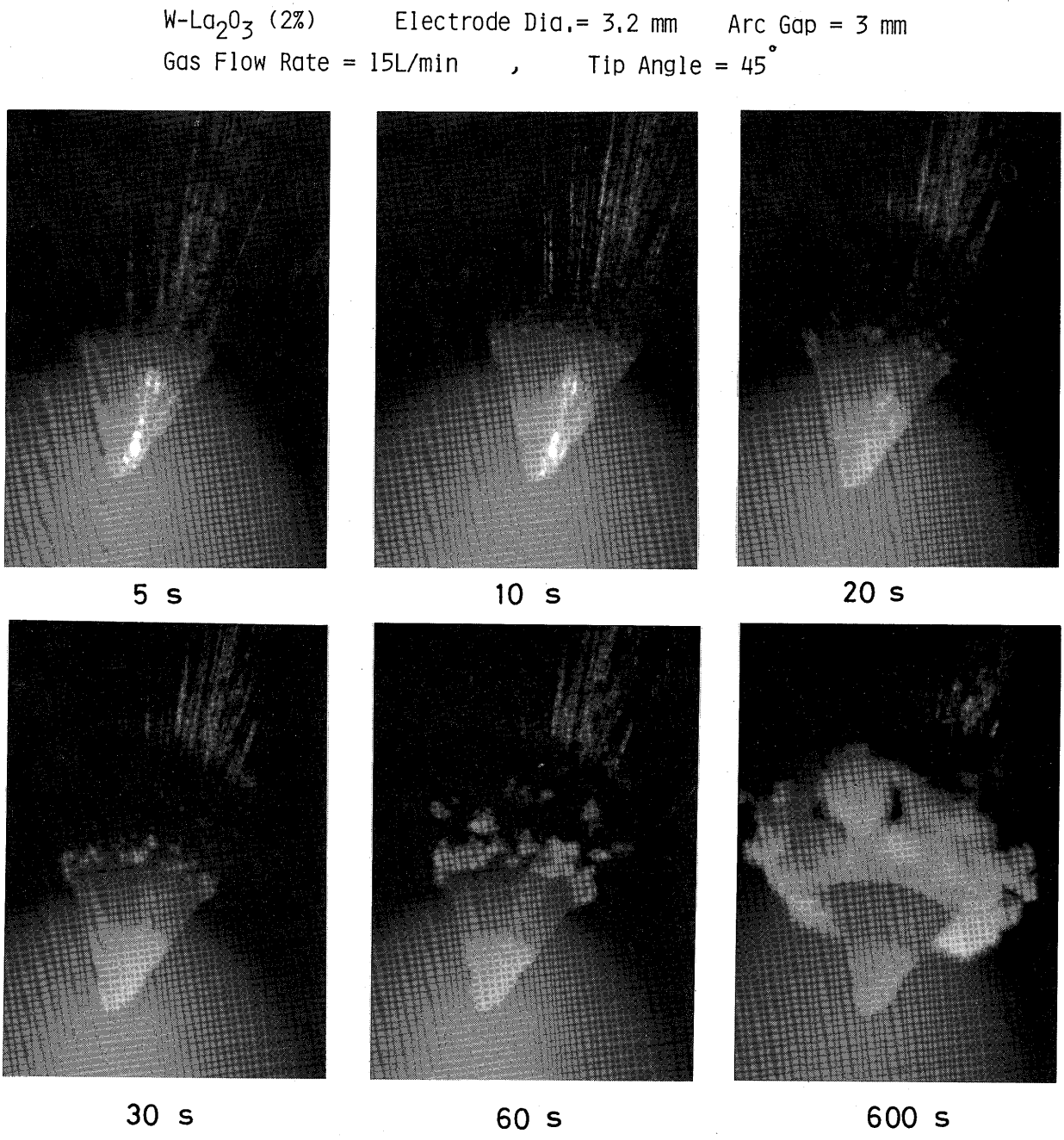

Fig. 5 Development of rim formation during arcing at 100A in argon and oxygen shielding gas.

$$\Sigma J_W = \frac{\bar{D}}{\Delta RT} \Sigma P_{W_xO_{2y}} \qquad (22)$$

Also, the partial pressures of all tungsten oxide species, the sum of these pressures at the surface are given in Table 1 as a function of the distance from electrode tip and the temperature relative to this distance. Based on that results it is obvious that, the decrease in oxidation and vaporization rates with increasing temperature results from a decrease in ΣP_W, since the term, $\bar{D}/\Delta RT$, in Equ. (22) changes very little with temperature.

(2) The intercept point between the flux at the electrode surface and maximum flux in vaccum is the point of vaporization cut-off. That means, below this point the boundary layer condition is no longer maintaned as explained before in the basic assumptions of calculation procedure.

4.5 Rim Formation Mechanism

Based on such data, the rim formation mechanism was thought as follows; due to the change of vaporization

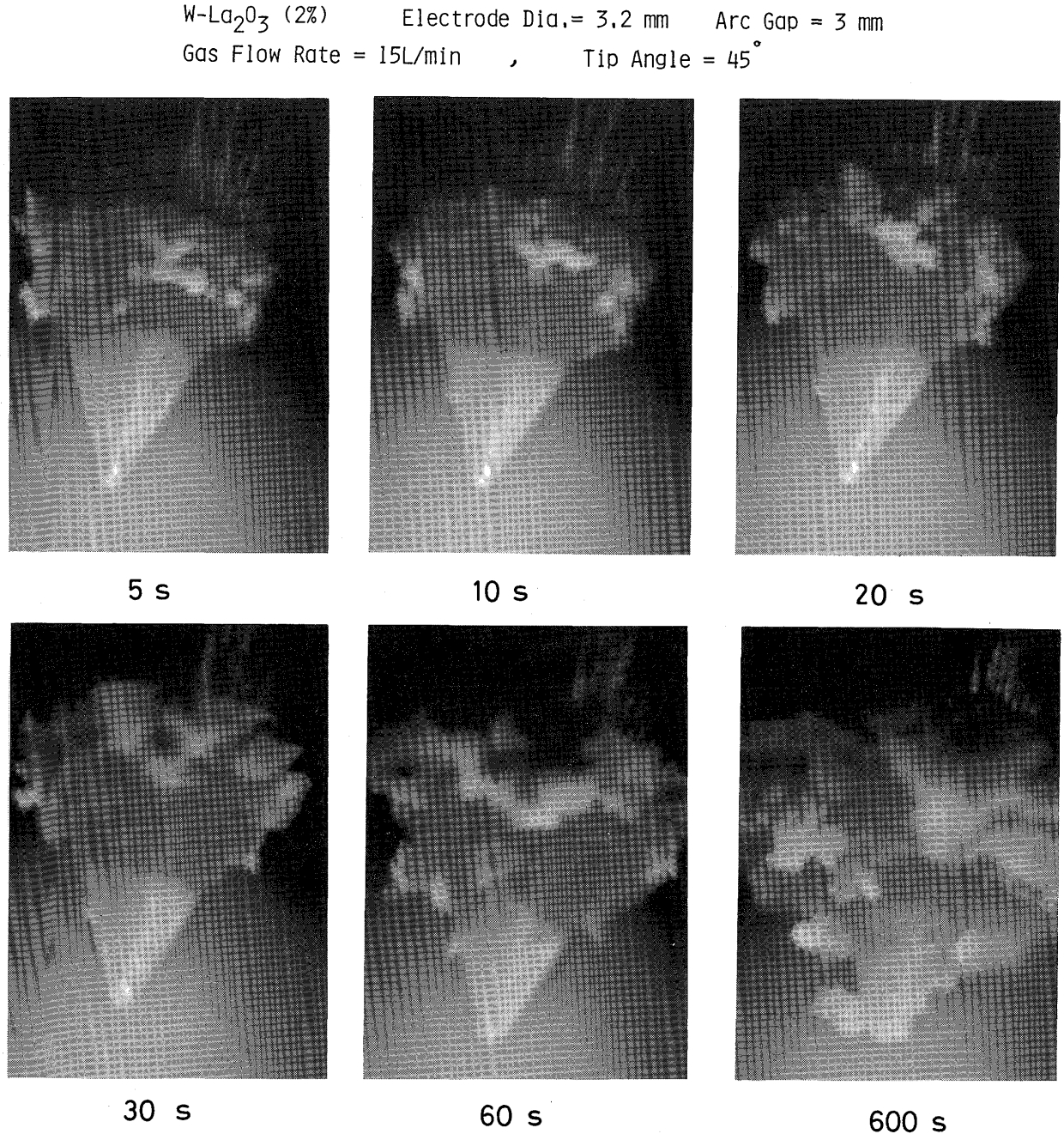

Fig. 6 Development of rim formation during arcing at 200A in argon and oxygen shielding gas.

rates along the electrode surface then there are regions have high vaporization rate while other regions have low vaporization rate. This occured through the longitudinal profil of boundary layer which is in parallel with the vertical axis of electrode.

Under the effect of gas stream, these oxides transfered along the electrode surface and concentrated until critical ratio was reached within the boundary layer, then condensation occured on the electrode surface forming rim.

Furthermore, the rim is formed at the point at which the boundary layer condition is no longer maintained and formation of liquid oxide layer is occured. The computed distance of this point from the electrode tip is 1.3 mm which is in reasonable agreement with the experimental results. Also, the area under that point has the same phenomena, but under the arc pressure this liquid oxide layer is pushed up to the rim region leaving the cathode area of the electrode free from deposition. According to that, this area can be considered as a second feader source of rim.

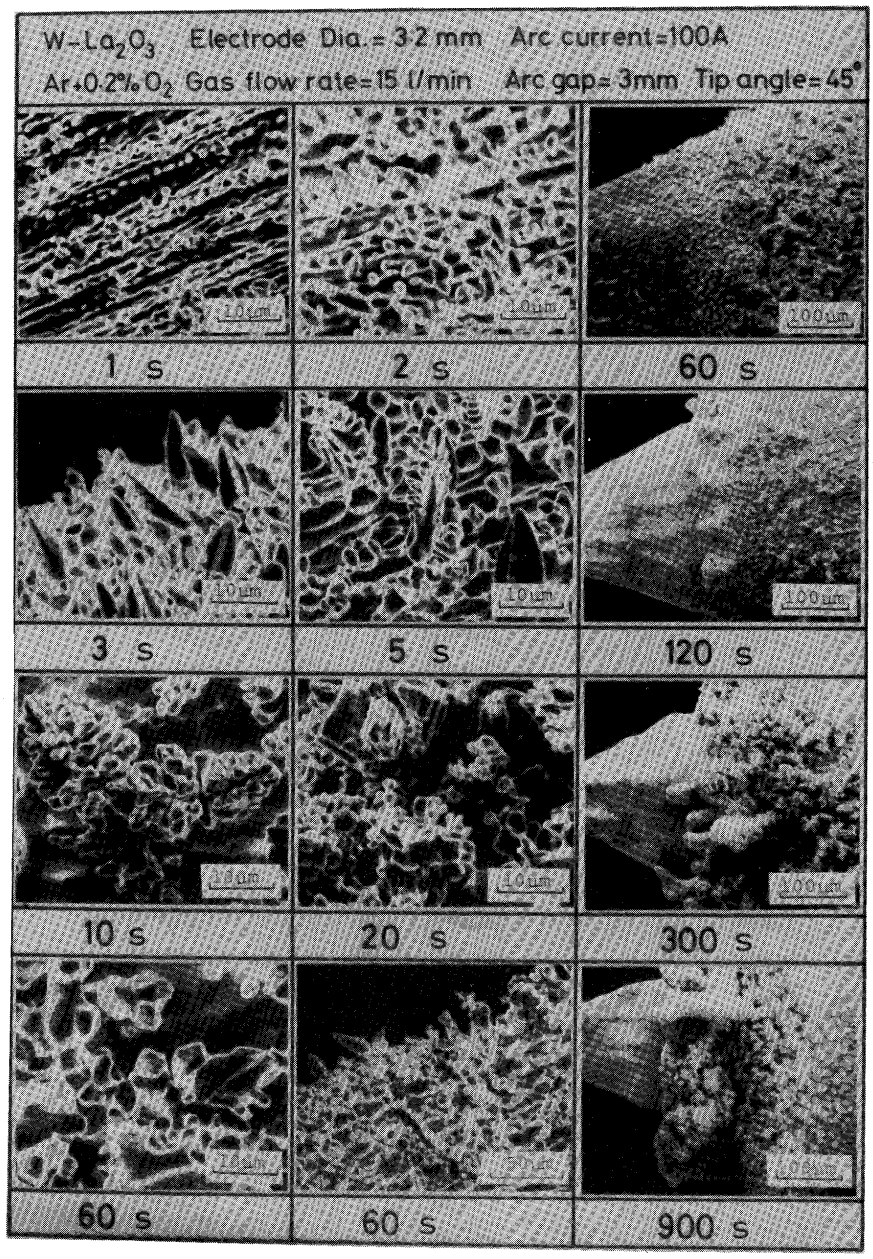

Fig. 7 SEM photographs of rim formation steps.

5. Conclusions

The main conclusions drawn from the experimental and theoretical datas are as follows:

(1) The presence of oxygen in shielding gas promot the rim formation accompanied with necking area just behined the rim.

(2) The size of rim and necking area is changed as a function of oxygen content and arcing time. Also, the rate formation of rim is depende on the arc current.

(3) The necking area formed due to the change of gas flow pattern from linear flow to circulation flow after the formation of rim. This circulation flow pattern increase the erosion rate at this area forming this necking area.

(4) The oxidation behaviour of tungsten electrodes is a function of arc current and shielding gas and changes significantly with arcing time.

(5) The rim structure is dendritic structure and consistes of tungsten, according to the results of EDX analysis.

(6) The rate of vaporization, generally, decreases with increasing temperature.

(7) The formation mechanism of rim was attributed to the vaporization, dessociation and deposition phenomenas of tungsten oxides which occured simultaneously along the electrode surface during arcing.

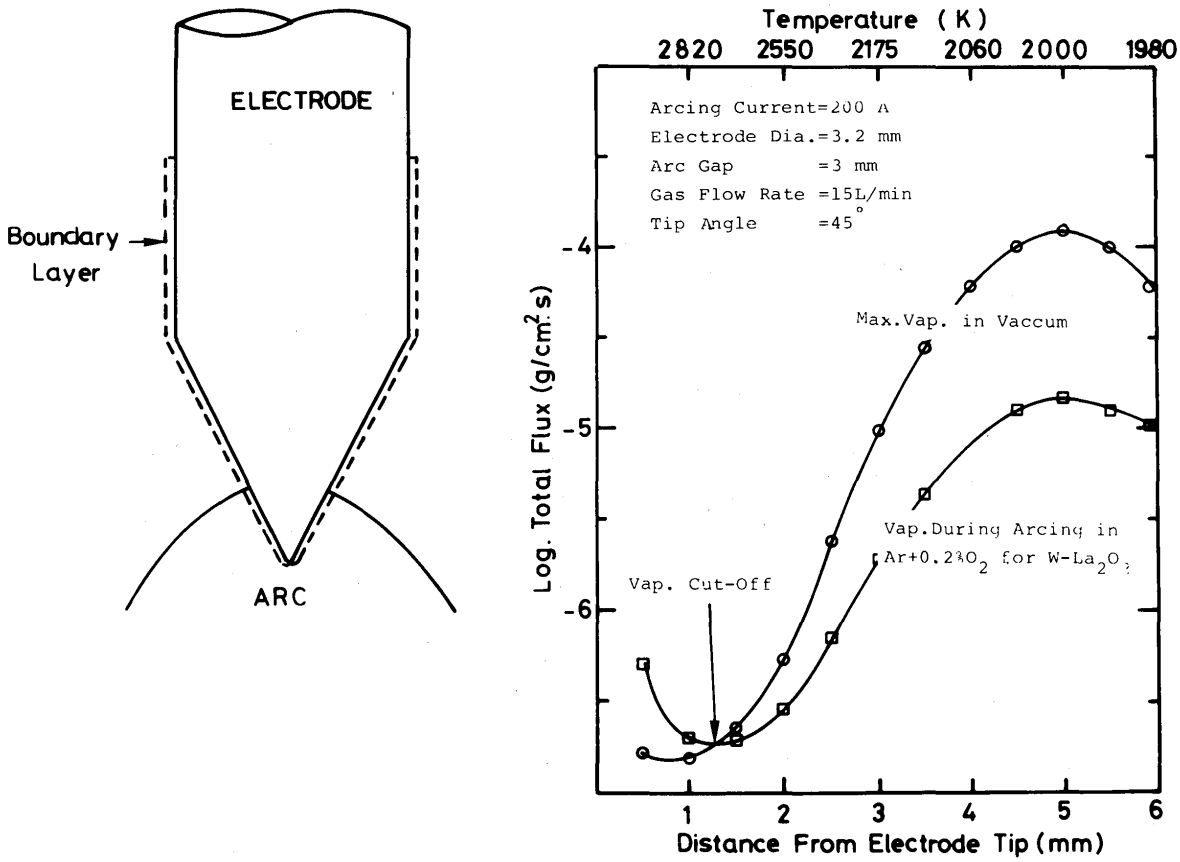

Fig. 8 Computed flux of tungsten oxides along the electrode surface.

Table 1 Partial pressure of tungsten oxides at the electrode surface.

Dist. (mm)	1	2	3	4	5	6
Temp. (K)	2820	2550	2175	2060	2000	1980
P_{WO}	0.364714^{-2}*	0.663421^{-2}	0.168791	0.576653	0.147451^{+1}	0.861655
P_{WO_2}	0.641007^{-8}	0.739096^{-9}	0.113395^{-8}	0.133402^{-8}	0.151038^{-8}	0.140679^{-8}
P_{WO_3}	0.241938^{-12}	0.168467^{-14}	0.142851^{-15}	0.559858^{-16}	0.273661^{-16}	0.412190^{-16}
$P_{W_2O_6}$	0.160162^{-26}	0.706480^{-32}	0.677772^{-36}	0.202209^{-37}	0.138112^{-38}	0.641499^{-38}
$\Sigma P_{W_xO_{2y}}$	3.64715^{-3}	6.634211^{-3}	0.168791	0.576653	1.47451	0.861655

*To be read as 0.364714×10^{-2}

References

1) F. Matsuda, M. Ushio and T. Kumagai, Trans. of JWRI, (1986), Vol. 15, No. 1, P. 13.
2) A.A. Sadek, M. Ushio and F. Matsuda, Trans. of JWRI, (1987), Vol. 16, No. 1, P. 195.
3) R.W. Bartlett, Trans. of Metall. Soc. of AIME, (1964), Vol. 230, P. 1097.
4) F.J. Harvey, Metall. Trans., (1973), Vol. 4, P. 1513.
5) E.T. Turkdogan, P. Grieveson and L.S. Darken, J. of Phys. Chem., (1963), Vol. 67, P. 1647.
6) E.T. Turkdogan, Trans. of Metall. Soc. of AIME, (1964), Vol. 230, P. 740.
7) F.J. Harvey, Metall. Trans., (1972), Vol. 3, P. 2973.
8) J.O. Hirschfelder, C.F. Curtiss and R.B. Bird, "Molecular Theory of Gases and Liquids", Jhon Wiley and Sons, Inc., New York, N.Y. (1954).
9) R.B. Bird, W.E. Stewart, E.N. Lightfoot, "Transport Phenomena Jhon Wiely and Sons, Inc., New York, (1960).
10) JANAF Thermochemical Tables, The Dow Chemical Company, Midland Michigan, (1963).
11) W. Frie, Z. Fur Physik, (1967), Vol. 201, P. 269.
12) F. Matsuda, M. Ushio and H. Fuji, Trans. of JWRI, (1987), Vol. 15, No. 2, P. 7.